



Influence of soil redox state on mercury sorption and reduction capacity

Mathieu Debure, Sylvain Grangeon, Jean-Charles Robinet, Benoît Madé, Ana María Fernández, Catherine Lerouge

► To cite this version:

Mathieu Debure, Sylvain Grangeon, Jean-Charles Robinet, Benoît Madé, Ana María Fernández, et al.. Influence of soil redox state on mercury sorption and reduction capacity. Science of the Total Environment, 2020, 707, pp.136069. 10.1016/j.scitotenv.2019.136069 . hal-02911790

HAL Id: hal-02911790

<https://brgm.hal.science/hal-02911790>

Submitted on 21 Dec 2021

HAL is a multi-disciplinary open access archive for the deposit and dissemination of scientific research documents, whether they are published or not. The documents may come from teaching and research institutions in France or abroad, or from public or private research centers.

L'archive ouverte pluridisciplinaire **HAL**, est destinée au dépôt et à la diffusion de documents scientifiques de niveau recherche, publiés ou non, émanant des établissements d'enseignement et de recherche français ou étrangers, des laboratoires publics ou privés.



Distributed under a Creative Commons Attribution - NonCommercial 4.0 International License

Influence of soil redox state on mercury sorption and reduction capacity.

Mathieu Debure^{1,*}, Sylvain Grangeon¹, Jean-Charles Robinet², Benoît Madé², Ana María Fernández³, Catherine Lerouge¹

¹ BRGM – French Geological Survey - 45060 Orléans - France.

² Andra, R&D Division, Transfer Migration Group, 92298 Châtenay-Malabry, France

³ CIEMAT, Dpto. Medio Ambiente, Avda./Complutense 40, 28040, Madrid, Spain

Abstract

We investigated the mechanisms of interactions between divalent aqueous Hg and rock samples originating from an outcropping rock formation, the Albian Tégulines Clay (France, Aube). Two solid samples collected at two different depths (7.7 and 21.2 m depth) in the rock formation were selected since, *in situ*, they had and were still experiencing contrasting redox conditions, and thus had different mineralogy with regards to the minerals containing redox-sensitive elements, in particular iron. The sample that was the closer to the surface was under oxidizing conditions and contained goethite and siderite, while the deeper one was under reducing conditions and had more siderite, together with pyrite and magnetite. The redox state of the samples was preserved throughout the present study by careful conditioning, preparation, and use them under O₂-free conditions. The two samples had similar affinity for Hg, with a retention coefficient (R_D) ranging between 10² and 10⁶ mol·kg⁻¹ when the aqueous Hg concentration ranged between 4.4 and 10⁷ ng·L⁻¹ with the lowest concentration for the highest R_D . However, the mechanisms of interaction differed. In the oxidized sample, no change in Hg redox state was observed, and the retention was due to reversible adsorption on the mineral phases (including organic matter). In contrast, upon interaction with the deeper and reduced sample, Hg was not only adsorbed on the mineral phases, but part of it was also reduced to dissolve elemental Hg. This reduction was attributed to magnetite and siderite and highlights the influence of mineralogy on the geochemical cycle of Hg.

* Corresponding author. E-mail address: m.debure@brgm.fr (M. Debure).

26

27 **Keywords:** *Tégulines Clay, redox environment, mercury speciation, volatilisation.*

28

33

34 **1. Introduction**

35 Hg is a metallic element that is toxic for many life forms, including bacteria, fungi, plants, and
36 mammals. The toxicity level depends upon several factors, including the dose, chemical speciation,
37 and duration and mode of exposure (Beckers and Rinklebe, 2017). It is generally agreed in the
38 literature that the most hazardous Hg form is methyl-mercury ($[\text{CH}_3\text{Hg}]^+$), because it is prone to bio-
39 accumulation and damages cells and organs. For example, methyl-mercury mainly damages the
40 nervous system of human while the ingestion of Hg(II) salts affects the kidneys. However, other Hg
41 forms are also toxic, although the mechanisms of toxicity differ. Therefore, understanding the
42 geochemical cycle of Hg in the environment, including where and how Hg can be mobilized or
43 accumulated, and under which chemical form, is fundamentally important.

44 When under its Hg(II) oxidation state, Hg can be adsorbed on several soil components, including the
45 generally most abundant ones, namely clay minerals such as illite, kaolinite and montmorillonite.
46 Several studies have also reported the retention of Hg(II) by organic matter and Fe(II)-bearing iron
47 oxides and manganese oxides (Beckers et al., 2019; Jiskra et al., 2014; Kerndorff and Schnitzer,
48 1980; Leterme and Jacques, 2015; Sklyberg, 2010). Additionally, it has been shown that sorption of
49 Hg(II) by these latter phases can involve the reduction of Hg(II) into Hg(0) (Charlet et al., 2002). This
50 raises the question of whether sorption experiments performed on soil samples can be interpreted in
51 terms of a simple retention phenomenon, if Hg speciation after the experiment is not determined. From
52 a more fundamental point of view, reduction of Hg(II) to Hg(0) by soils may have significant
53 implications for the understanding of the geochemical cycle of Hg. Indeed, because Hg(0) is gaseous
54 at ambient temperature and pressure and has a residence time in the atmosphere of ~ 1 y (Tokos et
55 al., 1998), it can be regarded as a global toxic chemical (Frohne et al., 2012; Kowalik et al., 2003;
56 Overesch et al., 2007; Rinklebe et al., 2010; Rinklebe et al., 2009).

57 Due to these strong implications, the release of Hg(0) from soils, and more generally the soil-air
58 exchange rates of Hg, has been the subject of numerous studies (Lindberg et al., 2002; Schlüter,
59 2000; Schroeder et al., 1989; Schroeder and Munthe, 1998; Zhang et al., 2003). It is observed that the
60 release of Hg depend mainly on soil temperature and water content (Gillis and Miller, 2000; Song and
61 Van Heyst, 2005; Zhang et al., 2003). This could be explained by the fact that increasing the soil water

saturation can promote the reduction of Hg(II) to Hg(0), and hence the potential volatilisation of Hg (Gillis and Miller, 2000; Johnson and Lindberg, 1995; Song and Van Heyst, 2005). However, despite these numerous studies, the role played by the individual soil components (e.g., organic matter or oxides) on the capacity of soil to reduce Hg(II) is currently poorly constrained. This study aims at contributing to a better understanding of Hg(II) reduction by soil.

The soil studied here, the Tégulines Clay (hereafter named sediment), had developed on an Albian sedimentary clay-rich formation that is located in the eastern part of the Paris basin. This geological formation is currently studied in France as a potential host for the storage of low-level long-lived (LL-LL) radioactive waste, which includes, in addition to radionuclides, toxic chemicals such as Hg (Lerouge et al., 2018). Such waste is mainly produced by the chemical industry (rare earth element extraction) and the clean-up of radioactively contaminated sites (former industrial plants, laboratories...). The behaviour of Hg in the Tégulines Clay was addressed to evaluate the fate of Hg from waste in the biosphere and its potential environmental impact. Due to its vicinity with the surface (~ 5 m), the Tégulines Clay is affected by weathering processes inducing fluctuations of redox conditions with depth (Debure et al., 2018; Lerouge et al., 2018). In addition, redox contrasts can be enhanced by the ground water table variations (water saturation and desaturation). Redox changes may affect the speciation of Hg and potentially its mobility through the rock layer, notably at the vicinity of the surface in the vadose zone. To achieve a better understanding of the mobility of Hg in such an environment, Tégulines Clay samples originating from two depths with distinct redox environments were considered to study the retention mechanisms of Hg. We focused especially on the sorption and reduction of Hg(II) on (or by) mineral surfaces. Therefore, the distribution of naturally occurring Hg amongst the different mineralogical components, and its retention coefficient (ratio of adsorbed to aqueous Hg) were determined. Then, the sorption of Hg(II) was studied by performing batch sorption/desorption tests, with specific attention paid to quantifying the reversibility/irreversibility and reduction phenomena. Finally, the retention processes of Hg were studied on the Tégulines Clay to assess the Hg mobility in function of the reducing capacity of the rock and its mineralogy.

2. Materials and methods

2.1. Context of the study and samples

2.1.1. Geological setting

The marine Gault Clay Formation consists of siliciclastic shales deposited from Middle to Upper Albian (Lower Cretaceous) on the Greensands formation. It outcrops as an 8–10 km wide and 80-km long band of terrane oriented NE-SW through the Aube Department, in the eastern part of the Paris Basin (France) (Amédéo et al., 2017; Lerouge et al., 2018). The stratotype of the Gault Clay defined in the Aube department consists of the Tégulines Clay (82 m) overlaid by the Brienne Marls (43 m). In the studied area, the thickness of the Tégulines Clay varies from 65-75 m to ~10 m. It is covered by thin (0.7 to 6 m thick) surficial layers of soil or alluvium. The Tégulines Clay are mainly composed of clay minerals (35-65 wt% including muscovite and/or illite, chlorite, kaolinite) associated with a quartz-feldspar silty fraction (18–58 wt%), and carbonates (0–30 wt%) (Lerouge et al., 2018). Accessory minerals include pyrite, celestite, and phosphates nodules in Tégulines Clay horizons experiencing reducing conditions ($E_h < 300$ mV, hereafter referred to as “reduced” horizons or samples) and gypsum, and iron oxides in weathered clay ($E_h > 300$ mV, hereafter referred to as “oxidized” horizons or samples). As the formation is subjected to weathering with the occurrence of oxidation phenomena, the mineralogy of the Tégulines Clay evolves with depth (Lerouge et al., 2018) and therefore influences the mobility of the traces (Debure et al. (2018) for further details).

Fig. 1. Magnified geological map of the area investigated in the eastern part of the Paris Basin (France) and location of the boreholes.

2.1.2. Sampling

In order to define the impact of weathering processes on Hg retention, two core samples (~400 to 600 g) were selected at two different depths. The two samples came from boreholes drilled through surficial formations and the Gault clay down to Greensands. The first one was collected at 7.70 m in the AUB 121 borehole (sample reference: AUB00976) and the second one at 21.20 m depth in the borehole AUB131 (sample reference: AUB00307) (Fig. 1). The samples AUB00976 and AUB00307 were considered to be representative of the oxidized and reduced zones, respectively. The drilling

mud was carefully removed from the core edges and then, the two samples were preserved in double layer aluminium bags under vacuum to prevent any additional oxidation just after coring. A part of the samples (~ 100 g) was freeze-dried to remove water, then milled in an agate mortar, and sieved at 100 µm in a glove box under a nitrogen atmosphere (see Debure et al. (2018) and Lerouge et al. (2018) for further details). The other part was used for pore water extraction with a squeezing technique (see section 2.2.3).

2.2. *Analytical technics and experiments*

2.2.1. *Bulk chemistry*

Total Fe content was assayed in the sediments through a modified 1,10-phenanthroline method (Hadi et al., 2013). In this two-steps method, Fe(II) content is quantified first by H₂SO₄/HF acid attack, and then measuring total Fe content by reducing all Fe present to Fe(II). Total organic carbon was quantified using a Jobin Yvon EMIE 820V carbon analyzer after acidic treatment of the sample to remove carbonates. The whole-rock bulk chemistry is available in Lerouge et al. (2018) and is not detailed in this study.

2.2.2. *Natural contents and distribution of Hg among phases in the Tégulines Clay*

Hg distribution among several chemical reservoirs was analysed by the means of sequential extractions that were performed on triplicates of each sample, in a glove box, following the method developed by Claret et al. (2010), modified after Tessier et al. (1979). The sequential extraction involved 4 steps (Table 1), which correspond to contacting the samples first with MgCl₂, then sodium acetate and acetic acid (buffered at pH 5), then NH₂OH, and finally H₂O₂ (at T = 85°C). The main mineralogical reservoirs that were targeted with these 4 steps were the interlayer space of clay minerals, calcite, Fe and Mn (oxyhydr-)oxides, and organic matter, respectively.

Table 1. Chemical extraction scheme for Hg fractionation highlighting the sequential extraction steps and mineralogical targets.

2.2.3. *Pore water extraction by squeezing*

Pore water was extracted from the samples using the squeezing technique from Fernández et al. (2014). A modification of the water sampling circuit was made to the squeezing system for extracting the pore water in anoxic conditions, preserving its redox state. The squeezing measurements were carried out only on the reduced sample, which was less exposed to atmospheric perturbations than the oxidized sample. The pore water was, therefore, not or less disturbed by rock oxidation. The mass of the core sample was measured before and after squeezing. The initial mass of core sample was 527 g. Extraction was carried out at 10 MPa over nine days and 18.6 mL of pore water were collected.

2.2.4. *Natural Hg content and lability, sorption and desorption experiments*

The synthetic pore water was prepared with boiled and outgassed Millipore Milli-Q® 18 MΩ·cm water and using CaSO₄·2H₂O, MgSO₄·7H₂O, KCl, NaCl, SrCl₂·6H₂O, Na₂SO₄ and NaHCO₃ salts (Supplementary Information A). Their purity was higher than 99 % and no Hg was detected. The preparation was performed in a glove box with an atmosphere close to field conditions, at equilibrium with carbonates (~100 kPa of N₂, ~1013 Pa of CO₂, O₂ < 0.1 Pa). The synthetic pore water chemistry was based on the pore water chemistry deduced from the geochemical modelling performed in Lerouge et al. (2018), following the guidelines proposed by Gaucher et al. (2009). Note that *In situ* pore water measured by squeezing (Lerouge et al., 2018) was consistent with the one synthetic one used here. Synthetic pore water was used in this study for the equilibration and “batch” sorption tests in order to avoid any mineral alteration, dissolution, or precipitation.

All the experiments were performed in a glove box under anoxic conditions to avoid any oxidation phenomenon. Once the pore water had been prepared, the desired volume was equilibrated in a polypropylene copolymer vial for at least 24 h, under agitation and with a suitable sediment mass. Afterwards, agitation was stopped, the solution was decanted for 30 min, and then the supernatant was sampled (~ 20 mL) and filtrated at 0.1 µm (PVDF).

Batch sorption experiments, conducted to determine the Hg distribution coefficients on rock powder, were mainly performed using a solid to liquid ratio, R_{SL}, of 5 g·L⁻¹. A R_{SL} of 2.5 g·L⁻¹ or 1 g·L⁻¹ was used for four experiments where the Hg concentration was 8.2 × 10⁻⁷ mol·L⁻¹, 9.4 × 10⁻⁷ mol·L⁻¹, 4.7 × 10⁻⁵ and 5.1 × 10⁻⁵ (Supplementary Information B).

The distribution coefficient (R_D) of any element (here, Hg) is the ratio between the concentration of the element in the solid phase (in $\text{mol}\cdot\text{kg}^{-1}$) and in the liquid phase (in $\text{mol}\cdot\text{L}^{-1}$), when equilibrium is assumed to be reached. This is expressed (equation 1) as:

$$R_D = \frac{C_{\text{sorb}}}{C_{\text{final}}} \quad (1)$$

Where R_D has for units $\text{L}\cdot\text{kg}^{-1}$, C_{sorb} is concentration of Hg sorbed on the sediment (in $\text{mol}\cdot\text{kg}^{-1}$) and C_{final} is the element concentration at equilibrium (in $\text{mol}\cdot\text{L}^{-1}$).

However, in most experiments, the concentration on the solid (C_{sorb}) is not measured directly, but inferred from the quantification of the concentration of the element of interest that has been removed from the solution by the solid. This concentration (in $\text{mol}\cdot\text{L}^{-1}$) must be related to the mass of solid in solution in order to quantify the corresponding concentration on the solid phase (in $\text{mol}\cdot\text{kg}^{-1}$), thus leading to equation 2:

$$R_D = \frac{(C_{\text{added}} - C_{\text{final}})}{R_{\text{SL}} C_{\text{final}}} \quad (2)$$

where C_{added} is the Hg concentration added in the retention experiments (in $\text{mol}\cdot\text{L}^{-1}$) and R_{SL} is the solid/liquid ratio in the experiment (in $\text{kg}\cdot\text{L}^{-1}$).

Mother solutions containing Hg were prepared with analytical grade salts (using HgCl_2). Then, an aliquot (from 1 to 10 mL depending of the experiments) was introduced into a vial containing the sediment suspension in order to reach the initial target concentration. The solution and the sediments were kept in contact for four days during the sorption tests and seven days during the desorption tests. The solution sampling method was the same as that described for the equilibration tests.

2.2.5. Analysis of the aqueous phases

The measurement of pH in batch solutions was carried out with a Mettler Toledo SevenMulti pH meter using NIST pH 1.7, 4, 7, and 9 buffers. Inductively coupled plasma atomic emission spectroscopy (ICP-AES, Jobin Yvon) or mass spectroscopy (ICP-MS, Thermo Fisher Scientific) was used to measure Ca, K, Mg, Na, and Si concentrations. Cl, SO_4 , S_2O_4 , Br, PO_4 and F were analysed by ionic chromatography (HPLC, Dionex). The elemental concentrations in solution were determined with a

relative uncertainty of 3 %. The samples were not acidified in order to avoid any Hg loss. After Hg measurement, the remaining solution was acidified with HNO₃ (10 µL at 10 %) prior to the solution analyse with ICP. Total Hg was at first measured by atomic fluorescence spectrometry, and then the speciation [Hg(II)/Hg(0)] was determined on selected samples by another technique described below.

2.2.6. *Mercury speciation*

All analytical procedures were conducted using ultra-clean sample handling to avoid laboratory contamination of low-level sample extracts and cross-contamination of high-level samples (Cossa and Gobeil, 2000). The aqueous sample was analysed for total Hg and Hg(0) by Au-amalgamation (EPA method 1631) and hydride generation-cryogenic trapping followed by cold vapour atomic fluorescence spectrometry (CVAFS) using a PSA mercury analyser (Millennium Merlin model) and a Tekran® mercury detector (2500 model), respectively, after conversion of all mercury species into Hg(0) (Bloom and Fitzgerald, 1988). The method is detailed in Hellal et al. (2015) and Cossa and Gobeil (2000) and is summarized in Supplementary Information C.

3. Results and discussion

3.1. *Mineralogy of Tégulines Clay samples and Hg distribution among the different phases*

The mineralogy of the Tégulines Clay samples studied here consisted mainly of clay minerals, quartz, feldspar, and calcite, together with minor dolomite/ankerite, siderite, pyrite and organic matter in the reduced sample and additional gypsum and iron (oxyhydr-)oxides in the oxidized sample (see Supplementary Information D and Debure et al. (2018)). The oxidized zones are characterized by the disappearance of pyrite and the presence of oxidation by-products such as goethite and gypsum while the reduced zones are characterized of the persistence of the minerals prone to oxidation such as pyrite and preserved glauconite. Since Hg has a strong affinity for organic matter and iron oxides (Harris-Hellal et al., 2011), its nature was specifically studied. In addition, the redox state of Fe was quantified.

During the H₂O₂ extraction step that targeted organic matter, sulfur was extracted. This could be interpreted as sulfur bound to the organic matter, or could be due to the fact that this chemical extraction also (partially) dissolved another component of the sample. In the first assumption, the

organic matter of the reduced sample (AUB00307) contained $(1800 \pm 133) \mu\text{g}\cdot\text{g}^{-1}$ of sulfur, while its sulfur content remained below the limit of quantification (of $1669 \mu\text{g}\cdot\text{g}^{-1}$) for the oxidized sample (AUB00976). However, and although it could not be ruled out that this sulfur originated for example from organic matter thiols, it must be noted that the reduced sample contained pyrite whose limited oxidation during the H_2O_2 extraction step could have been responsible for the presence of sulfur in solution. The hypothesis of pyrite oxidation is supported by the fact that Fe was also extracted during this step (see below). Thus, no clear conclusion can be drawn about potential differences between the organic matter from both samples, and the reactivity of the organic matter component toward Hg was expected to be roughly similar for both samples. Indeed, the reduced sample contained a slightly higher content of organic matter (0.73 wt% vs 0.58 wt%), but the difference was too slight and within the range of the measurements on other boreholes (Lerouge et al., 2018) to induce a measurable difference in reactivity between the two samples.

The total Fe concentration of the reduced sample (3.81 %) was slightly higher than that of the oxidized sample (2.46 %). The bulk Fe(II)/Fe(III) ratio was 82 % for the reduced sample, and 17 % for the oxidized sample, supporting the destabilization of Fe(II)-bearing minerals and formation of iron hydroxides at shallow depth. The sequential extraction showed that in both samples (Fig. 2 and Supplementary Information E) the residual fraction was the main Fe reservoir: it contained 74 % of total iron in the reduced sample and 95 % in the oxidized sample. The Fe-bearing minerals present in the residual fraction (Table D-1) were pyrite (FeS_2 , that contain ~46 % Fe) and the clay minerals (illite/mica and illite-smectite mixed-layer minerals: 2 to 5 % Fe, chlorite: up to ~16 % Fe). No exchangeable Fe could be detected. The fraction associated with carbonates represented 0.6 % of total Fe in the reduced sample and 0.3 % in the oxidized sample. The two extraction steps targeting Fe and Mn (oxyhydr-)oxides and the organic matter led to higher Fe recovery in the reduced sample than in the oxidized one. In the reduced sample, the first step made it possible to extract $(6.8 \pm 0.5) \%$ of the total Fe and the second step $(18.3 \pm 1.3) \%$ of the total Fe, compared to respectively $(0.7 \pm 0.1) \%$ of the total Fe in the first and $(4.5 \pm 0.2) \%$ of the total Fe in the second for the oxidized sample. These results could be interpreted as (1) the reduced sample containing more Fe(II)-bearing Fe (oxyhydr-)oxides than the oxidized one or (2) the organic matter in the reduced sample containing more Fe than that of the oxidized sample. However, as for sulfur, Fe extracted during the H_2O_2 extraction step could be attributed to limited pyrite oxidation. In order to account for this possible pyrite

oxidation, the total Fe extracted during the H_2O_2 step was thus corrected from hypothetical pyrite oxidation by subtracting a Fe content equal to half that of the sulfur extracted in the same step (as the structural formula of pyrite is FeS_2). Still, the quantity of Fe contained in the organic matter and iron (oxyhydr-)oxides components were higher in the reduced sample (Fig. 2).

Fig. 2. Total Fe (%) extracted by the different steps of the sequential extraction protocol, corrected from hypothetical partial pyrite oxidation during Step 4. Uncorrected data are available in Supplementary Information E (Sample oxidized: AUB976; sample reduced: AUB307).

An attempt was made to quantify the natural Hg distribution from sequential extraction leachates. However, given the low natural Hg concentration in the samples, Hg concentration remained below the detection limit ($25 \text{ ng}\cdot\text{g}^{-1}$) at all extraction steps and for all samples, except for the H_2O_2 step of the reduced samples, where $(3.9 \pm 1.9) \text{ ng}\cdot\text{g}^{-1}$ Hg was extracted. It is nevertheless noteworthy that the amount extracted remained close to the detection limit, and no clear conclusion regarding the natural Hg distribution could be drawn from these sequential extractions. The total Hg content measured on the bulk sample was $(20 \pm 6) \text{ ng}\cdot\text{g}^{-1}$ for the reduced sample and $(19 \pm 6) \text{ ng}\cdot\text{g}^{-1}$ for the oxidized sample.

3.2. Chemical composition of pore water extracted by squeezing and natural distribution coefficient of Hg in the Tégulines Clay

Pore water was extracted from the reduced sample by the squeezing technique at 10 MPa, following Debure et al. (2018); see Table 2. The pH of the extracted pore water was 7.7. The $\text{S}_2\text{O}_3^{2-}$ concentration ($0.20 \text{ mmol}\cdot\text{L}^{-1}$) was consistent with the reduced state of the sample (redox potential $< 198 \text{ mV}$) but highlighted in the meantime a slight sulfide oxidation (Boulegue and Michard, 1979; Kurth et al., 2015; Vairavamurthy et al., 1993). Both Fe and Al were systematically below the detection limit ($0.01 \text{ mmol}\cdot\text{L}^{-1}$). Hg concentration was $0.015 \text{ }\mu\text{mol}\cdot\text{L}^{-1}$, similar to that of As ($0.010 \text{ }\mu\text{mol}\cdot\text{L}^{-1}$) and Cr ($0.029 \text{ }\mu\text{mol}\cdot\text{L}^{-1}$).

Table 2. Pore water chemistry measured after squeezing of the reduced sample (cations and anions in $\text{mmol}\cdot\text{L}^{-1}$ and trace elements in $\mu\text{mol}\cdot\text{L}^{-1}$).

Since Hg could be measured both in the pore water and in the solid phase of the reduced sample, the natural distribution coefficient ($R_{D,Nat}$), which quantifies the solid-solution partitioning, could be calculated as follows:

$$R_{D,Nat} = \frac{C_{sediment,Nat}}{C_{porewater}} \quad (3)$$

where $C_{Pore\ water}$ is the Hg pore water concentration (in $\text{mol}\cdot\text{L}^{-1}$, Table 2), and $C_{sediment,Nat}$ is the concentration of Hg in the sediments (in $\text{mol}\cdot\text{kg}^{-1}$) determined by sequential extractions (section 3.1). The $R_{D,Nat}$ of Hg was found to be $(6.5 \pm 1) \times 10^3 \text{ L}\cdot\text{kg}^{-1}$ for the reduced samples, and $(6.1 \pm 1) \times 10^3 \text{ L}\cdot\text{kg}^{-1}$ for the oxidized samples, which is consistent with the $R_{D,Nat}$ reported for several types of soils, sediments, and suspended matter of lakes and rivers (Fig. 3 – data from Bloom et al., (1999), Drexel et al., (2002) and Hurley et al., (1998) (see also Bone et al., (2007) and Hammerschmidt and Fitzgerald, (2004)).

3.3. Sorption experiments on Tégulines Clay

The R_D obtained in batch experiments ranged from $\sim 1.2 \times 10^3$ to $\sim 1 \times 10^6 \text{ L}\cdot\text{kg}^{-1}$ for the reduced sample and from $\sim 1 \times 10^2$ to $\sim 9 \times 10^5 \text{ L}\cdot\text{kg}^{-1}$ for the oxidized sample, for equilibrium Hg concentrations that ranged from 4.4 to $1 \times 10^7 \text{ ng}\cdot\text{L}^{-1}$. The R_D increased when equilibrium Hg concentration decreased, in agreement with the river, soil and sediment literature data (Fig. 3). The fact that batch R_D values were in agreement with $R_{D,Nat}$ means that the study of the retention phenomenon in these batch experiments could provide insights into the mechanisms occurring in the natural setting and over long time scales. Note that the Hg R_D is generally higher for the reduced sample (Fig. 3) although strict point-by-point comparison could not be performed since Hg equilibrium concentrations differed in the two different datasets (oxidized or reduced samples).

According to literature data, Hg has a particular affinity for iron oxides and organic matter, in particular for the thiols (Beckers et al., 2019; Jiskra et al., 2014; Kerndorff and Schnitzer, 1980; Leterme and Jacques, 2015; Skyllberg, 2010). As goethite is present as trace concentration in the Tégulines Clay (Lerouge et al., 2018), geochemical calculations (Allison et al., 1991; Parkhurst and Appelo, 2013) were performed to determine whether this mineral could quantitatively account for the observed R_D (Fig. 4). If the sample had consisted of pure goethite, modelling indicates that the R_D could not have

exceeded $10^4 \text{ L}\cdot\text{kg}^{-1}$ if the solution had contained only NaCl and $5\cdot 10^{-9} \text{ mol}\cdot\text{L}^{-1}$ of Hg (Fig. 4.a and Supplementary Information F). This R_D value is in the range of the observed R_D values but does not consider the actual pore water chemistry. Introducing it in the modelling reduced the predicted R_D to $1.6 \times 10^2 \text{ L}\cdot\text{kg}^{-1}$ (Fig. 4.b) because Ca competed with Hg for sorption. This value is two orders of magnitude lower than the observed R_D value and does not consider the fact that goethite was not a major mineral, but a trace component. Thus, goethite could not account for the observed R_D , and another sorbing phase and (or) retention mechanism had to be considered. Since they are a major component of the samples, clays certainly contribute to the Hg R_D , but they are ruled out as the main Hg sorbing phase because their retention capacity is lower than that of Fe (oxyhydr-)oxides, even when sorption occurs at pH 3 where clay sorption capacity is enhanced whereas that of Fe (oxyhydr-)oxides is strongly reduced (Barrow and Cox, 1992; Cruz-Guzman et al., 2003; Farrah and Pickering, 1978). Finally, and as discussed above, the organic matter could also be responsible for the observed R_D . However, a difference in R_D was observed between the two samples, while the organic matter content was similar (section 3.1). Consequently, and although organic matter certainly contributed significantly to Hg retention, another phenomenon responsible for the difference in R_D between the reduced and oxidized samples had to be considered. To determine whether this additional process was irreversible (e.g., incorporation in a mineral phase or Hg reduction), the reversibility of sorption was tested on the samples with the highest Hg concentration ($4.70 \times 10^{-5} \text{ mol}\cdot\text{L}^{-1}$). The reduced sample released in solution around 1 % of the total Hg initially sorbed, while 30 % was released by the oxidized sample (Table 3). This evidenced the presence of an irreversible process whose extent depended on the sample. To further investigate the nature of this process, the speciation of the aqueous Hg remaining in solution after the sorption experiments was investigated.

Between 60 and 93 % of Hg was present as Hg(0) in the solution in contact with the reduced sample and was thus suspected to be reduced upon interaction with the solid phase, while only 1 % of Hg was reduced upon contact with the oxidized sample (Fig. 5). In addition, the lower the initial concentration, the higher the proportion of Hg(0) in the final solution. Indeed, almost half the remaining Hg was Hg(II) in the experiments with the highest initial Hg concentration ($5.1 \times 10^{-5} \text{ mol}\cdot\text{L}^{-1}$), while it represented only 7 % in the experiment with the lowest initial concentration ($8.2 \times 10^{-8} \text{ mol}\cdot\text{L}^{-1}$). This results suggests that the element or the phase at the origin of this reduction was depleted and therefore, we could assume that the reducing capacity of the sediment is lower than $5.1 \times 10^{-6} \text{ mol}\cdot\text{g}^{-1}$. Both organic

matter (e.g. Allard and Arsenie, 1991; Ravichandran, 2004) and Fe(II)-bearing Fe (oxyhydr-)oxides such as magnetite or green rust (O'Loughlin et al., 2003; Wiatrowski et al., 2009) are able to reduce Hg(II) to Hg(0) and could be responsible for the Hg reduction observed in our experiments involving the reduced sample. The organic matter content in the two samples is similar and, therefore, only a difference in terms of its nature would have explained the higher Hg(II) reduction on the reduced sample. Such a difference was not observed in this study (section 3.1). In addition, Hg(II) reduction by organic matter is a photochemical reaction that requires UV radiation (Costa and Liss, 2000; Costa and Liss, 1999; Faïn et al., 2007) - although humic acids can induce Hg reduction in the dark (Gu et al., 2011). As the present experiments were conducted in a glove box with no direct solar irradiation and thus probably in the absence of UV radiation, the occurrence of photochemical reactions is unlikely in the present study.

Therefore, we propose that Fe(II)-bearing minerals led to the Hg(II) reduction. The amount of Fe(II) available in the solid-phase was consistent with this assumption (section 3.1). The carriers of Fe(II) are glauconite (~8 wt%), pyrite (~0.4 wt%), siderite (~0.3 wt%) and magnetite (traces, only detected by low-temperature magnetic remanence methods) in the clay formation (Debure et al., 2018; Lerouge et al., 2018). Siderite can reduce Hg (Ha et al., 2017). However, with a size of the siderite in the Tégulines Clay of ~40 µm (Lerouge et al. (2018)), it has a surface area of ~0.07 m²·g⁻¹. Ha et al. (2017) reported that 70 % of 5.8 × 10⁻⁸ mol of Hg was reduced by 0.1 g of siderite with a surface area of 126.1 m²·g⁻¹. This surface area and this content are both three orders of magnitude higher than the surface area and the siderite content in the Tégulines Clay. Furthermore, even if siderite had been able to reduce a large part of the lowest used concentration (2.7 × 10⁻⁹ mol), it seems unlikely that it would have reduced 60 % (Fig. 5) of the highest concentration of Hg added (2.0 × 10⁻⁶ mol). We conclude from this analysis that siderite alone cannot quantitatively explain the observed Hg reduction. Magnetite was detected in the reduced sample but not in the oxidized sample and can reduce Hg(II) (Wiatrowski et al., 2009), presumably according to the following equation:



As magnetite was only present in the reduced sample at trace concentration (< 0.1 %), one can wonder if trace amounts were sufficient quantitatively to account for the observed Hg(II) reduction. In the case of total reduction, a suspension having an R_{SL} of 0.010 kg·L⁻¹ would have required 2.04 × 10⁻⁵

moles·g⁻¹ of Fe(II) to reduce 5.1×10^{-5} mol·L⁻¹ of Hg(II) into Hg(0). The total Fe concentration in the reduced sample was 3.81 % (of which 82 % is Fe(II)) (section 3.1), that is 6.82×10^{-4} mol·g⁻¹ and thus 5.60×10^{-4} mol·g⁻¹ of Fe(II). Consequently, ~7.3 % of the Fe(II) (6.0 % of the total Fe) would have been sufficient to quantitatively account for the reduction of Hg(II) to Hg(0) observed in the present experiments, i.e. 4.3×10^{-6} mol of iron and therefore 1.4×10^{-6} mol of magnetite (Fe₃O₄). Such an amount is in agreement with the fact that the sum of pyrite and magnetite contents represent ~10 % of the total Fe, with pyrite being the most abundant of the two minerals (Lerouge et al., 2018). Finally, it is worth noting that a mercury reduction on glauconite cannot be ruled out. Indeed, no dedicated experiments investigating the sorption and reduction of Hg on these clay minerals are available in the literature to our knowledge. Therefore, the accessible Fe(II) in glauconite is not known and its influence on the reduction of Hg cannot be assessed without dedicated experiments that are beyond the scope of this study.

In the oxidized sample, the Fe(II) is lower. In addition, the presence of Fe(III) iron hydroxides such as goethite or ferrihydrite prevent the Hg(II) reduction and promote adsorption as the preferred pathway to Hg removal from the solution (Gabriel and Williamson, 2004; Vernon and Bonzongo, 2014). In addition, the vadose zone is subject to water saturation/desaturation cycles that favour oxygen diffusion and limit reduction processes. Indeed, oxidative weathering impedes electron transfer. Therefore, magnetite cannot be argued to explain the retention in the oxidized experiments and sorption on iron oxides proved insufficient to explain R_D. Among the other solids available, organic matter is able to complex with Hg(II) and inhibits its reduction by reduced minerals (Jiskra et al., 2014). Such a process is consistent with the R_D coefficient of Hg calculated especially for the oxidized sample (Fig. 3 and Supplementary Information B). Indeed, no or little Hg(0) (< 1.5 %) was detected in the solution contacting the oxidized sample, thus discarding volatilisation as the main process explaining the high retention coefficient.

Fig. 3. Comparison of the R_{D,Nat} and R_D acquired on the oxidized and reduced sample with values reported for several types of soils, sediments, and suspended matter of lakes and rivers (Aastrup et al., 1991; Åkerblom et al., 2008; Berzas et al., 2003; Hines et al., 2000; Lyon et al., 1997; Paraquetti et al., 2004; Suchanek et al., 1998; Sultan et al., 2011; Thompson-Roberts et al., 1999). The crosses and pluses represent the R_D calculated with the quantification limit of

Hg ($7 \times 10^{-11} \text{ mol}\cdot\text{L}^{-1}$), therefore representing the lowest threshold of the R_D value. The stars and minuses represent the desorption data.

Fig. 4. Theoretical Hg retention coefficient on ferrihydrite considering that the whole sediment is ferrihydrite (Hfo-1g), 10 % is ferrihydrite (Hfo-100mg), 1 % is ferrihydrite (Hfo-10mg) and 0.1 % is ferrihydrite (Hfo-1mg). The quantity of Hg added is $5 \times 10^{-5} \text{ mol}\cdot\text{L}^{-1}$. This concentration is the maximum concentration added in the experiments. a) The chemistry of the water is only composed of Na and Cl ($1.47 \text{ mmol}\cdot\text{L}^{-1}$), b) the pore water chemistry is considered. The calculations were performed with the PhreeqC code (Parkhurst and Appelo, 2013) and the Minteq database version 4 (Allison et al., 1991). The quantity of weak binding sites is 2.4×10^{-3} moles, the quantity of strong binding sites is 6×10^{-5} moles, the specific surface area is $600 \text{ m}^2\cdot\text{g}^{-1}$, the weight of the sample varies from 1 mg to 1 g in agreement with theoretical values given for ferrihydrite by Parkhurst and Appelo (2013) and the pH is fixed at 7.5, which is the value of the pore water.

Table 3. Sorption and desorption coefficients calculated at the initial Hg concentration of $4.70 \times 10^{-5} \text{ mol}\cdot\text{L}^{-1}$ on the oxidized and reduced samples.

Fig. 5. Determination of the speciation of Hg after the retention experiment on the oxidized sample (AUB00976) and on the reduced sample (AUB00307). a. The initial Hg concentration was $8 \times 10^{-8} \text{ mol}\cdot\text{L}^{-1}$; b. the initial Hg concentration was $5.1 \times 10^{-5} \text{ mol}\cdot\text{L}^{-1}$. The lower the initial concentration, the higher the reduction percentage.

3.4. Implications for Hg retention by clay rocks

Both oxidized and reduced Tégulines Clay have a strong affinity for Hg but only reduced Tégulines Clay can reduce Hg(II) into Hg(0). This reduction, which could possibly occur in many clay rocks containing Fe(II)-bearing Fe (oxyhydr-)oxides and minerals, could have here induced an overestimation of the quantity of Hg(II) that can be adsorbed by the solid phase, since part of the

Hg(0) could have been lost by volatilisation prior to measurement. However, this effect was probably of limited importance for most samples, since the sum of Hg(0) and Hg(II) concentrations measured during the speciation experiments was in good agreement with the total Hg concentration used for the R_D calculation (Supplementary Information B, Table B-3 and B-4). The only sample for which discrepancy was observed is related to the experiment that involved the reduced sample and the highest initial Hg concentration ($5.1 \times 10^{-5} \text{ mol}\cdot\text{L}^{-1}$). In these experimental conditions, the total Hg concentration measured in the experiment that aimed at determining the Hg R_D was about one order of magnitude lower than the sum of Hg(0) and Hg(II) measured in the experiment that aimed at determining Hg speciation in solution. The total Hg concentration was measured a short time after the end of the experiment that may have led to Hg outgassing. Indeed, this value is consistent with the Hg(II) concentration measured in this experiment. This result highlights the need to perform the analytical measurements as quickly as possible in such a reducing soil system.

Among the parameters that could influence the fate of Hg, thiosulfate in the pore water (Table 2) may also reduce Hg(II) to Hg(0), or more likely influence its fate through its complexation with Hg (Hellal et al., 2015; Johannesson and Neumann, 2013). Either way, it could thus result in the formation of a strong complex like those observed for sulfides (Moreno et al., 2004; Wang et al., 2012), increasing the stability of Hg in solution and therefore its transport. However, here, the thiosulfate concentration was low and this mechanism was certainly of minor importance. In addition, the Gault pore water is outside the predominance area of the complexes composed of Hg and S (Supplementary Information G). Hg was also found to sorb on quartz (Bonnissel-Gissinger et al., 1999; Tiffreau et al., 1995) and clays (Cruz-Guzman et al., 2003), which are a major constituent of the Tégulines Clay, especially at shallow depths (see Supplementary Information D and (Debure et al., 2018; Lerouge et al., 2018)). No correlation was found in this study between the quartz content and Hg retention. This was most likely due to the lower affinity of Hg for quartz than for iron hydroxides and organic matter. Among the available clays, illite, kaolinite and smectite have a lower affinity for Hg than iron hydroxides (Cruz-Guzman et al., 2003; Gabriel and Williamson, 2004; Jiskra et al., 2014) but the behaviour (sorption and reduction) of Hg in contact with glauconite is poorly known.

Finally, the fate of Hg in the Tégulines Clay depends on organic compounds, soil redox conditions, and the redox state of iron in minerals. In Fe-reducing sediments such as preserved Tégulines Clay, the reduction of Hg(II) by solid-phase Fe(II) may occur in anoxic groundwater while in oxic surficial

sediments reduced minerals are less common, with the exception of magnetite (Wiatrowski et al., 2009), and thus Hg(II) reduction is limited. However, green rusts that form in anthropogenic soils can transform into magnetite upon reduction due to the variation of the water table (Sumoondur et al., 2008; Trolard and Bourrie, 2008) and finally affect the speciation of Hg and therefore its mobility. In reduced and saturated sediments, the Hg(II) reduction promotes Hg mobilization as Hg(0) but prevents the formation of methyl Hg (MeHg) that normally forms from a Hg(II) precursor (Colombo et al., 2013; Fitzgerald et al., 1991). The former is usually found in groundwater with high levels of Fe(II) (Barringer et al., 2005). Therefore, Fe cycling impacts the mobility and fate of Hg especially in the vadose zone where the water table varies (interface between oxidative and reductive conditions) (Johannesson and Neumann, 2013).

4. Conclusions

The behaviour of Hg, its sorption, reduction and volatilisation have been investigated on the Tégulines Clay, a clay-rich rock formation that outcrops in the eastern part of the Paris Basin. The retention of Hg was affected by the clay mineralogy, and in particular the reducing capacity of the samples. In such a system, Hg can be volatilised due to reduction phenomena initiated by sorption of Hg(II). The reduction was more effective in the reduced sample than in the oxidized sample due to the highest content of Fe(II)-bearing phases. Fe(II) acts as an electron donor in the reaction, leading to the reduction of Hg(II) into Hg(0). The main phase expected to be responsible for Hg(II) sorption-reduction is magnetite. Hg(0) can then be volatilised (when a gas phase exists) leading to a decrease in the Hg concentration in the system. Volatilisation phenomena could explain the low natural Hg content measured during the sequential extraction. On the other hand, the presence of an Fe(III)-bearing phase, such as iron hydroxides in the oxidized sample, is associated with a high retention capacity of Hg(II) in the rock. In addition, organic matter can contribute to the retention of Hg with a higher quantity of sulfur groups (thiol) in the organic matter of the reduced samples. Finally, the sorption capacity of the clay minerals (even lower than Fe (oxyhydr-)oxides) increases Hg retention both in the reduced and oxidized samples. Due to weathering processes (mainly driven by the percolation of dissolved oxygen from the surface) the redox of Tégulines Clay evolves leading then to different phenomena governing the retention of Hg. The presence of reduced phases preserved from weathering promotes the reduction of Hg(II) into Hg(0). In addition, the formation of green rusts in

anthropogenic soils and its possible transformation in magnetite upon reduction will influence the fate of Hg. Indeed, groundwater and sub-surface water variations generate redox oscillations favourable to (a)biotic reduction processes. Therefore, the soil is a complex environment, both because of the diversity of the mineral phases that compose it, and because of the exacerbated redox fluctuations at the interface between unsaturated and saturated zones. These oscillations promote (a)biotic reduction processes that impact the distribution and retention of Hg. The present study assess and quantify the impact of the sediment mineralogy on the mobilisation of Hg. However, the mobility of Hg(0) depends then on the water saturation of the rock with an expected lower migration under saturated conditions. Therefore, it is imperative to understand how these alternations influence the geochemistry of Hg(II) via sorption/desorption on formed/dissolved phases. In addition, competition between sorption and volatilisation may occur on some phases (glauconite) with both sites that can sorb mercury and Fe(II) that can reduce it. The understanding of all these processes will finally help to determine and assess the Hg cycling in environment.

Acknowledgements

This research was financially supported by the BRGM–Andra scientific partnership (TOGAULT Project). We also gratefully acknowledge Jennifer Hellal for giving us the possibility to use her mercury analyzer to determine the speciation. Thibault Conte (BRGM) is also acknowledged for his help with analytical matters. We would like to thank Sally Ferguson (Alba Traduction) for English language editing. We thank the two anonymous reviewers for the constructive comments that improved the quality of this study.

500

501 **References**

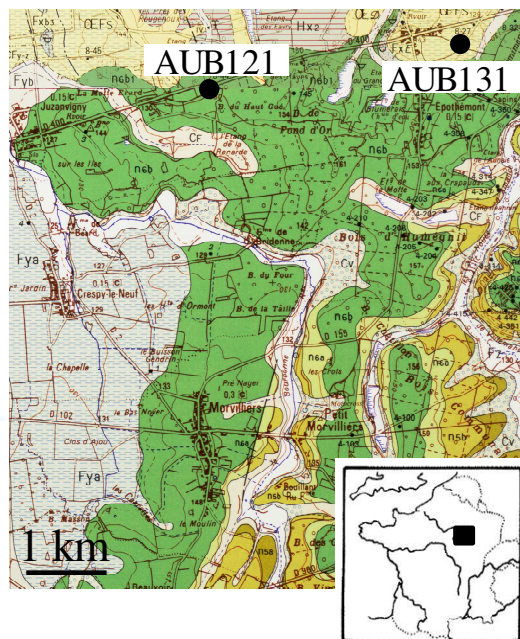
- 502 Aastrup M, Johnson J, Bringmark E, Bringmark I, Iverfeldt Å. Occurrence and transport of mercury
503 within a small catchment area. *Water Air & Soil Pollution* 1991; 56: 155-167.
- 504 Åkerblom S, Meili M, Bringmark L, Johansson K, Kleja DB, Bergkvist B. Partitioning of Hg between
505 solid and dissolved organic matter in the humus layer of boreal forests. *Water, air, and soil*
506 *pollution* 2008; 189: 239-252.
- 507 Allard B, Arsenie I. Abiotic reduction of mercury by humic substances in aquatic system — an
508 important process for the mercury cycle. *Water Air & Soil Pollution* 1991; 56: 457-464.
- 509 Allison JD, Brown DS, Novo-Gradac KJ. MINTEQA2/PRODEFA2, a geochemical assessment model
510 for environmental systems: version 3.0 user's manual: Environmental Research Laboratory,
511 Office of Research and Development, US ..., 1991.
- 512 Amédéo F, Matrimon B, Deconinck J-F, Huret E, Landrein P. Les forages de Juzanvigny (Aube, France):
513 litho-biostratigraphie des formations du Barrémien à l'Albien moyen dans l'est du bassin de
514 Paris et datations par les ammonites. *Geodiversitas* 2017; 39: 185-212.
- 515 Barringer JL, Szabo Z, Kauffman LJ, Barringer TH, Stackelberg PE, Ivahnenko T, et al. Mercury
516 concentrations in water from an unconfined aquifer system, New Jersey coastal plain. *Science*
517 *of the Total Environment* 2005; 346: 169-183.
- 518 Barrow NJ, Cox VC. The Effects of Ph and Chloride Concentration on Mercury Sorption .1. By
519 Goethite. *Journal of Soil Science* 1992; 43: 295-304.
- 520 Beckers F, Awad YM, Beiyuan J, Abridata J, Mothes S, Tsang DCW, et al. Impact of biochar on
521 mobilization, methylation, and ethylation of mercury under dynamic redox conditions in a
522 contaminated floodplain soil. *Environment International* 2019; 127: 276-290.
- 523 Beckers F, Rinklebe J. Cycling of mercury in the environment: Sources, fate, and human health
524 implications: A review. *Critical Reviews in Environmental Science and Technology* 2017; 47:
525 693-794.
- 526 Berzas JN, García LB, Rodríguez RM-D. Distribution of mercury in the aquatic environment at
527 Almadén, Spain. *Environmental pollution (Barking, Essex: 1987)* 2003; 122: 261-271.
- 528 Bloom N, Fitzgerald WF. Determination of volatile mercury species at the picogram level by low-
529 temperature gas chromatography with cold-vapour atomic fluorescence detection. *Analytica*
530 *Chimica Acta* 1988; 208: 151-161.
- 531 Bloom NS, Gill GA, Cappellino S, Dobbs C, McShea L, Driscoll C, et al. Speciation and Cycling of
532 Mercury in Lavaca Bay, Texas, Sediments. *Environmental Science & Technology* 1999; 33: 7-
533 13.
- 534 Bone SE, Charette MA, Lamborg CH, Gonneea ME. Has submarine groundwater discharge been
535 overlooked as a source of mercury to coastal waters? *Environmental science & technology*
536 2007; 41: 3090-3095.
- 537 Bonnissel-Gissinger P, Alnot M, Lickes J-P, Ehrhardt J-J, Behra P. Modeling the adsorption of mercury
538 (II) on (hydr) oxides II: α -FeOOH (goethite) and amorphous silica. *Journal of colloid and*
539 *interface science* 1999; 215: 313-322.

- 540 Boulegue J, Michard GIL. Sulfur Speciations and Redox Processes in Reducing Environments.
541 Chemical Modeling in Aqueous Systems. 93. AMERICAN CHEMICAL SOCIETY, 1979, pp.
542 25-50.
- 543 Charlet L, Bosbach D, Peretyashko T. Natural attenuation of TCE, As, Hg linked to the heterogeneous
544 oxidation of Fe(II): an AFM study. *Chemical Geology* 2002; 190: 303-319.
- 545 Claret F, Lerouge C, Laurieux T, Bizi M, Conte T, Ghestem JP, et al. Natural iodine in a clay formation:
546 Implications for iodine fate in geological disposals. *Geochimica et Cosmochimica Acta* 2010;
547 74: 16-29.
- 548 Colombo MJ, Ha J, Reinfelder JR, Barkay T, Yee N. Anaerobic oxidation of Hg(0) and methylmercury
549 formation by *Desulfovibrio desulfuricans* ND132. *Geochimica et Cosmochimica Acta* 2013;
550 112: 166-177.
- 551 Cossa D, Gobeil C. Mercury speciation in the lower St. Lawrence Estuary. *Canadian Journal of*
552 *Fisheries and Aquatic Sciences* 2000; 57: 138-147.
- 553 Costa M, Liss P. Photoreduction and evolution of mercury from seawater. *Science of The Total*
554 *Environment* 2000; 261: 125-135.
- 555 Costa M, Liss PS. Photoreduction of mercury in sea water and its possible implications for Hg⁰ air–
556 sea fluxes. *Marine Chemistry* 1999; 68: 87-95.
- 557 Cruz-Guzman M, Celis R, Hermosin MC, Leone P, Negre M, Cornejo J. Sorption-desorption of lead (II)
558 and mercury (II) by model associations of soil colloids. *Soil Science Society of America*
559 *Journal* 2003; 67: 1378-1387.
- 560 Debure M, Tournassat C, Lerouge C, Madé B, Robinet J-C, Fernández AM, et al. Retention of arsenic,
561 chromium and boron on an outcropping clay-rich rock formation (the Tégulines Clay, eastern
562 France). *Science of The Total Environment* 2018; 642: 216-229.
- 563 Drexel RT, Haitzer M, Ryan JN, Aiken GR, Nagy KL. Mercury(II) Sorption to Two Florida Everglades
564 Peats: Evidence for Strong and Weak Binding and Competition by Dissolved Organic Matter
565 Released from the Peat. *Environmental Science & Technology* 2002; 36: 4058-4064.
- 566 Faïn X, Grangeon S, Bahlmann E, Fritsche J, Obrist D, Dommergue A, et al. Diurnal production of
567 gaseous mercury in the alpine snowpack before snowmelt. *Journal of Geophysical Research:*
568 *Atmospheres* 2007; 112.
- 569 Farrah H, Pickering WF. The sorption of mercury species by clay minerals. *Water Air & Soil Pollution*
570 1978; 9: 23-31.
- 571 Fernández AM, Sánchez-Ledesma DM, Tournassat C, Melón A, Gaucher EC, Astudillo J, et al.
572 Applying the squeezing technique to highly consolidated clayrocks for pore water
573 characterisation: Lessons learned from experiments at the Mont Terri Rock Laboratory.
574 *Applied Geochemistry* 2014; 49: 2-21.
- 575 Fitzgerald WF, Mason R, Vandal G. Atmospheric cycling and air-water exchange of mercury over mid-
576 continental lacustrine regions. *Water Air & Soil Pollution* 1991; 56: 745-767.
- 577 Frohne T, Rinklebe J, Langer U, Laing GD, Mothes S, Wennrich R. Biogeochemical factors affecting
578 mercury methylation rate in two contaminated floodplain soils. *Biogeosciences* 2012; 9: 493-
579 507.
- 580 Gabriel M, Williamson D. Principal Biogeochemical Factors Affecting the Speciation And Transport of
581 Mercury through the terrestrial environment. *Environmental Geochemistry and Health* 2004;
582 26: 421-434.

- 583 Gaucher EC, Tournassat C, Pearson FJ, Blanc P, Crouzet C, Lerouge C, et al. A robust model for
584 pore-water chemistry of clayrock. *Geochimica et Cosmochimica Acta* 2009; 73: 6470-6487.
- 585 Gillis AA, Miller DR. Some local environmental effects on mercury emission and absorption at a soil
586 surface. *Science of the Total Environment* 2000; 260: 191-200.
- 587 Gu B, Bian Y, Miller CL, Dong W, Jiang X, Liang L. Mercury reduction and complexation by natural
588 organic matter in anoxic environments. *Proceedings of the National Academy of Sciences*
589 2011; 108: 1479-1483.
- 590 Ha J, Zhao X, Yu R, Barkay T, Yee N. Hg (II) reduction by siderite (FeCO₃). *Applied geochemistry*
591 2017; 78: 211-218.
- 592 Hadi J, Tournassat C, Ignatiadis I, Greneche JM, Charlet L. Modelling CEC variations versus structural
593 iron reduction levels in dioctahedral smectites. Existing approaches, new data and model
594 refinements. *Journal of colloid and interface science* 2013; 407: 397-409.
- 595 Hammerschmidt CR, Fitzgerald WF. Geochemical controls on the production and distribution of
596 methylmercury in near-shore marine sediments. *Environmental Science & Technology* 2004;
597 38: 1487-1495.
- 598 Harris-Hellal J, Grimaldi M, Garnier-Zarli E, Bousserhine N. Mercury mobilization by chemical and
599 microbial iron oxide reduction in soils of French Guyana. *Biogeochemistry* 2011; 103: 223-
600 234.
- 601 Hellal J, Guédron S, Hugué L, Schäfer J, Laperche V, Joulain C, et al. Mercury mobilization and
602 speciation linked to bacterial iron oxide and sulfate reduction: A column study to mimic
603 reactive transfer in an anoxic aquifer. *Journal of Contaminant Hydrology* 2015; 180: 56-68.
- 604 Hines ME, Horvat M, Faganeli J, Bonzongo J-CJ, Barkay T, Major EB, et al. Mercury biogeochemistry
605 in the Idrija River, Slovenia, from above the mine into the Gulf of Trieste. *Environmental*
606 *research* 2000; 83: 129-139.
- 607 Hurley J, Krabbenhoft D, Cleckner L, Olson M, Aiken G, Rawlik P, Jr. System controls on the aqueous
608 distribution of mercury in the northern Florida Everglades. *Biogeochemistry* 1998; 40: 293-
609 311.
- 610 Jiskra M, Saile D, Wiederhold JG, Bourdon B, Björn E, Kretzschmar R. Kinetics of Hg(II) Exchange
611 between Organic Ligands, Goethite, and Natural Organic Matter Studied with an Enriched
612 Stable Isotope Approach. *Environmental Science & Technology* 2014; 48: 13207-13217.
- 613 Johannesson KH, Neumann K. Geochemical cycling of mercury in a deep, confined aquifer: Insights
614 from biogeochemical reactive transport modeling. *Geochimica et Cosmochimica Acta* 2013;
615 106: 25-43.
- 616 Johnson D, Lindberg S. The biogeochemical cycling of Hg in forests: alternative methods for
617 quantifying total deposition and soil emission. *Mercury as a Global Pollutant*. Springer, 1995,
618 pp. 1069-1077.
- 619 Kerndorff H, Schnitzer M. Sorption of metals on humic acid. *Geochimica et Cosmochimica Acta* 1980;
620 44: 1701-1708.
- 621 Kowalik C, Kraft J, Einax JW. The situation of the German Elbe tributaries—Development of the loads
622 in the last 10 years. *Acta hydrochimica et hydrobiologica* 2003; 31: 334-345.
- 623 Kurth JM, Dahl C, Butt JN. Catalytic Protein Film Electrochemistry Provides a Direct Measure of the
624 Tetrathionate/Thiosulfate Reduction Potential. *Journal of the American Chemical Society*
625 2015; 137: 13232-13235.

- 626 Lerouge C, Robinet J-C, Debure M, Tournassat C, Bouchet A, Fernández AM, et al. A Deep Alteration
627 and Oxidation Profile in a Shallow Clay Aquitard: Example of the Tégulines Clay, East Paris
628 Basin, France. *Geofluids* 2018; 20.
- 629 Leterme B, Jacques D. A reactive transport model for mercury fate in contaminated soil—sensitivity
630 analysis. *Environmental Science and Pollution Research* 2015; 22: 16830-16842.
- 631 Lindberg SE, Zhang H, Vette AF, Gustin MS, Barnett MO, Kuiken T. Dynamic flux chamber
632 measurement of gaseous mercury emission fluxes over soils: part 2—effect of flushing flow
633 rate and verification of a two-resistance exchange interface simulation model. *Atmospheric*
634 *Environment* 2002; 36: 847-859.
- 635 Lyon B, Ambrose R, Rice G, Maxwell C. Calculation of soil-water and benthic sediment partition
636 coefficients for mercury. *Chemosphere* 1997; 35: 791-808.
- 637 Moreno FN, Anderson CW, Stewart RB, Robinson BH. Phytoremediation of mercury-contaminated
638 mine tailings by induced plant-mercury accumulation. *Environmental Practice* 2004; 6: 165-
639 175.
- 640 O'Loughlin EJ, Kelly SD, Kemner KM, Csencsits R, Cook RE. Reduction of AgI, AuIII, CuII, and HgII
641 by FeII/FeIII hydroxysulfate green rust. *Chemosphere* 2003; 53: 437-446.
- 642 Overesch M, Rinklebe J, Broll G, Neue H-U. Metals and arsenic in soils and corresponding vegetation
643 at Central Elbe river floodplains (Germany). *Environmental Pollution* 2007; 145: 800-812.
- 644 Paraquetti HHM, Ayres GA, De Almeida MD, Molisani MM, De Lacerda LD. Mercury distribution,
645 speciation and flux in the Sepetiba Bay tributaries, SE Brazil. *Water research* 2004; 38: 1439-
646 1448.
- 647 Parkhurst DL, Appelo CAJ. Description of Input and Examples for PHREEQC Version 3—a Computer
648 Program for Speciation, Batch-reaction, One-dimensional Transport, and Inverse
649 Geochemical Calculations., 2013.
- 650 Ravichandran M. Interactions between mercury and dissolved organic matter—a review.
651 *Chemosphere* 2004; 55: 319-331.
- 652 Rinklebe J, During A, Overesch M, Du Laing G, Wennrich R, Stärk H-J, et al. Dynamics of mercury
653 fluxes and their controlling factors in large Hg-polluted floodplain areas. *Environmental*
654 *Pollution* 2010; 158: 308-318.
- 655 Rinklebe J, During A, Overesch M, Wennrich R, Stärk H-J, Mothes S, et al. Optimization of a simple
656 field method to determine mercury volatilization from soils—examples of 13 sites in floodplain
657 ecosystems at the Elbe River (Germany). *Ecological Engineering* 2009; 35: 319-328.
- 658 Schlüter K. evaporation of mercury from soils. An integration and synthesis of current knowledge.
659 *Environmental Geology* 2000; 39: 249-271.
- 660 Schroeder W, Munthe J, Lindqvist O. Cycling of mercury between water, air, and soil compartments of
661 the environment. *Water, Air, and Soil Pollution* 1989; 48: 337-347.
- 662 Schroeder WH, Munthe J. Atmospheric mercury—an overview. *Atmospheric environment* 1998; 32:
663 809-822.
- 664 Skyllberg U. Mercury biogeochemistry in soils and sediments. *Developments in Soil Science*. 34.
665 Elsevier, 2010, pp. 379-410.
- 666 Song X, Van Heyst B. Volatilization of mercury from soils in response to simulated precipitation.
667 *Atmospheric Environment* 2005; 39: 7494-7505.

- 668 Suchanek T, Mullen L, Lamphere B, Richerson PJ, Woodmansee C, Slotton D, et al. Redistribution of
669 mercury from contaminated lake sediments of Clear Lake, California. *Water, Air, and soil*
670 *pollution* 1998; 104: 77-102.
- 671 Sultan K, Shazili NA, Peiffer S. Distribution of Pb, As, Cd, Sn and Hg in soil, sediment and surface
672 water of the tropical river watershed, Terengganu (Malaysia). *Journal of hydro-environment*
673 *Research* 2011; 5: 169-176.
- 674 Sumoondur A, Shaw S, Ahmed I, Benning L. Green rust as a precursor for magnetite: an in situ
675 synchrotron based study. *Mineralogical Magazine* 2008; 72: 201-204.
- 676 Tessier A, Campbell PGC, Bisson M. Sequential extraction procedure for the speciation of particulate
677 trace metals. *Analytical Chemistry* 1979; 51: 844-851.
- 678 Thompson-Roberts ES, Pick FR, Hall GE. Total Hg in water, sediment, and four species of aquatic
679 macrophytes in the St. Lawrence River, near Cornwall, Ontario. *Journal of Great Lakes*
680 *Research* 1999; 25: 294-304.
- 681 Tiffreau C, Lützenkirchen J, Behra P. Modeling the adsorption of mercury (II) on (hydr) oxides: I.
682 Amorphous iron oxide and α -quartz. *Journal of Colloid and Interface Science* 1995; 172: 82-
683 93.
- 684 Tokos JJ, Hall Bo, Calhoun JA, Prestbo EM. Homogeneous gas-phase reaction of Hg with H₂O₂, O₃,
685 CH₃I, AND (CH₃)₂S: Implications for atmospheric Hg cycling. *Atmospheric Environment*
686 1998; 32: 823-827.
- 687 Trolard F, Bourrie G. Geochemistry of green rusts and fougérite: a reevaluation of Fe cycle in soils.
688 *Advances in Agronomy* 2008; 99: 227-288.
- 689 Vairavamurthy A, Manowitz B, Luther III G, Jeon Y. Oxidation state of sulfur in thiosulfate and
690 implications for anaerobic energy metabolism. *Geochimica et Cosmochimica Acta* 1993; 57:
691 1619-1623.
- 692 Vernon JD, Bonzongo J-CJ. Volatilization and sorption of dissolved mercury by metallic iron of
693 different particle sizes: Implications for treatment of mercury contaminated water effluents.
694 *Journal of Hazardous Materials* 2014; 276: 408-414.
- 695 Wang J, Feng X, Anderson CWN, Wang H, Zheng L, Hu T. Implications of Mercury Speciation in
696 Thiosulfate Treated Plants. *Environmental Science & Technology* 2012; 46: 5361-5368.
- 697 Wiatrowski HA, Das S, Kukkadapu R, Ilton ES, Barkay T, Yee N. Reduction of Hg(II) to Hg(0) by
698 Magnetite. *Environmental Science & Technology* 2009; 43: 5307-5313.
- 699 Zhang H, Lindberg S, Gustin M, Xu X. Toward a better understanding of mercury emissions from soils.
700 *Biogeochemistry of Environmentally Important Trace Elements* 2003; 835: 246-261.
- 701



Aerial deposited silty soil

- OEs Loessal silts
- OEs Loamy clay to loamy sand caprock

Alluvial formations (above the bottom of the Aube valley)

- Fz Alluvium: gravel, silt, peat
- Fz1, Fz2, Fz3: stepped alluvial terraces
- Fyb Brienne plain (Fy)
- Fyb: base +5 to 7 m (Weichselian)
- Fya: base +8 to 10 m (Eemian)

Old alluvial formations (Voire valley)

- Hx2 Loamy clay caprock covering alluvial sands (Middle to recent Pleistocene)

Shelves and hillsides

- CV Colluviums: clay loams (Upper Pleistocene - Holocene)
- Cf

Cretaceous

- neb Gault clay – Tégulines Clay (Lower and middle Albian)
- neb1 Tégulines Clay, chalky and silty clays (Middle Albian) and their covering loamy clay caprock
- n6a Green sands (Lower Albian)
- n5b Quartz sands (Upper Aptian)
- n5a Plicatules Clay (Lower Aptian)

Fig. 1. Magnified geological map of the area investigated in the eastern part of the Paris Basin (France) and location of the boreholes.

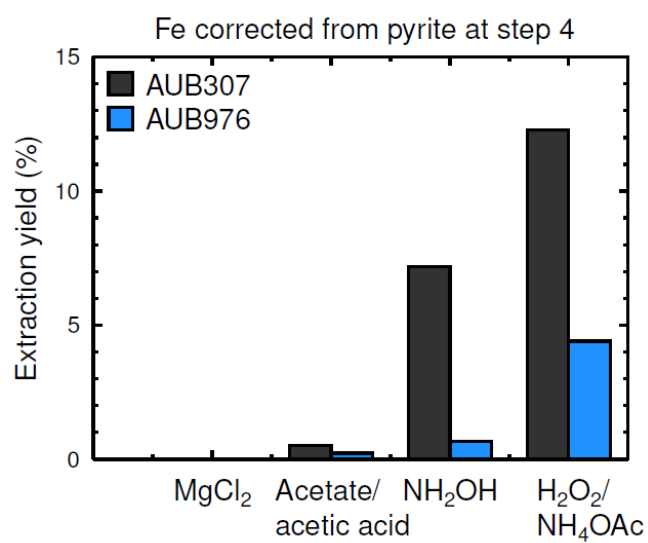


Fig. 2. Total Fe (%) extracted by the different steps of the sequential extraction protocol, corrected from hypothetical partial pyrite oxidation during Step 4. Uncorrected data are available in Supplementary Information E (Sample oxidized: AUB976; sample reduced: AUB307).

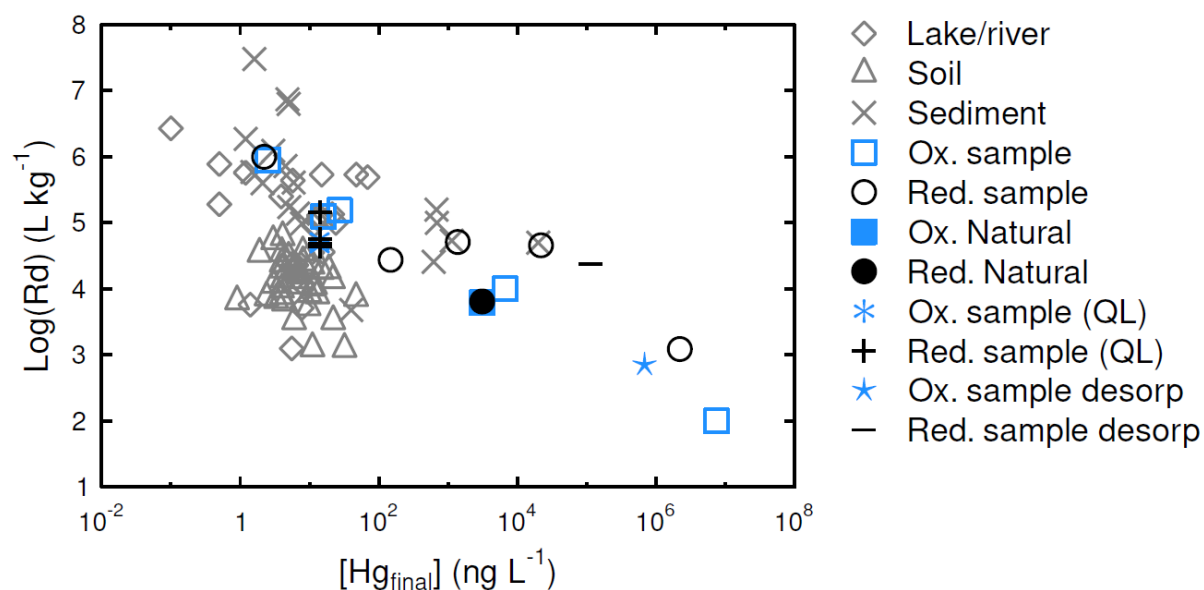


Fig. 3. Comparison of the $R_{D,Nat}$ and R_D acquired on the oxidized and reduced sample with values reported for several types of soils, sediments, and suspended matter of lakes and rivers (Aastrup et al., 1991; Åkerblom et al., 2008; Berzas et al., 2003; Hines et al., 2000; Lyon et al., 1997; Paraquetti et al., 2004; Suchanek et al., 1998; Sultan et al., 2011; Thompson-Roberts et al., 1999). The crosses and pluses represent the R_D calculated with the quantification limit of Hg ($7 \times 10^{-11} \text{ mol}\cdot\text{L}^{-1}$), therefore representing the lowest threshold of the R_D value. The stars and minuses represent the desorption data.

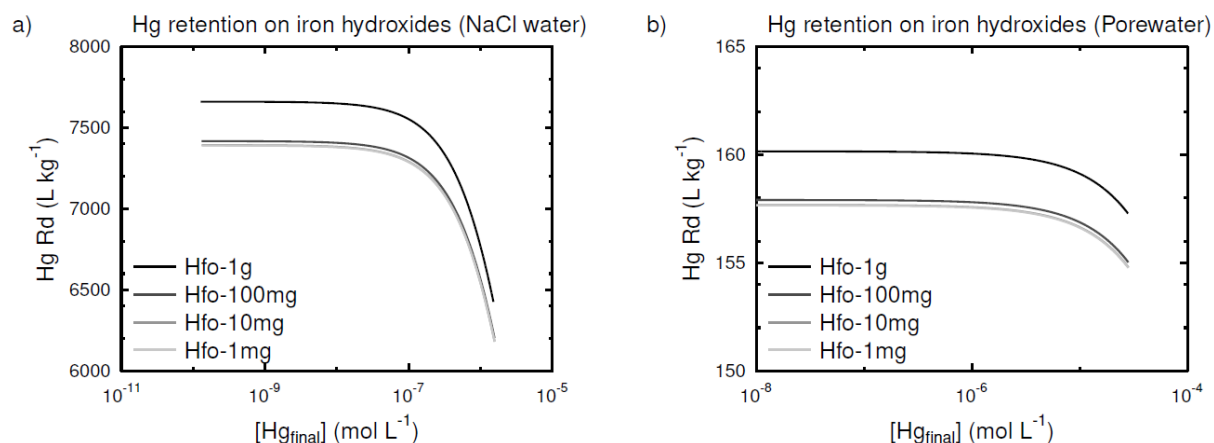


Fig. 4. Theoretical Hg retention coefficient on ferrihydrite considering that the whole sediment is ferrihydrite (Hfo-1g), 10 % is ferrihydrite (Hfo-100mg), 1 % is ferrihydrite (Hfo-10mg) and 0.1 % is ferrihydrite (Hfo-1mg). The quantity of Hg added is $5 \times 10^{-5} \text{ mol} \cdot \text{L}^{-1}$. This concentration is the maximum concentration added in the experiments. a) The chemistry of the water is only composed of Na and Cl ($1.47 \text{ mmol} \cdot \text{L}^{-1}$), b) the pore water chemistry is considered. The calculations were performed with the PhreeqC code (Parkhurst and Appelo, 2013) and the Minteq database version 4 (Allison et al., 1991). The quantity of weak binding sites is 2.4×10^{-3} moles, the quantity of strong binding sites is 6×10^{-5} moles, the specific surface area is $600 \text{ m}^2 \cdot \text{g}^{-1}$, the weight of the sample varies from 1 mg to 1 g in agreement with theoretical values given for ferrihydrite by Parkhurst and Appelo (2013) and the pH is fixed at 7.5, which is the value of the pore water.

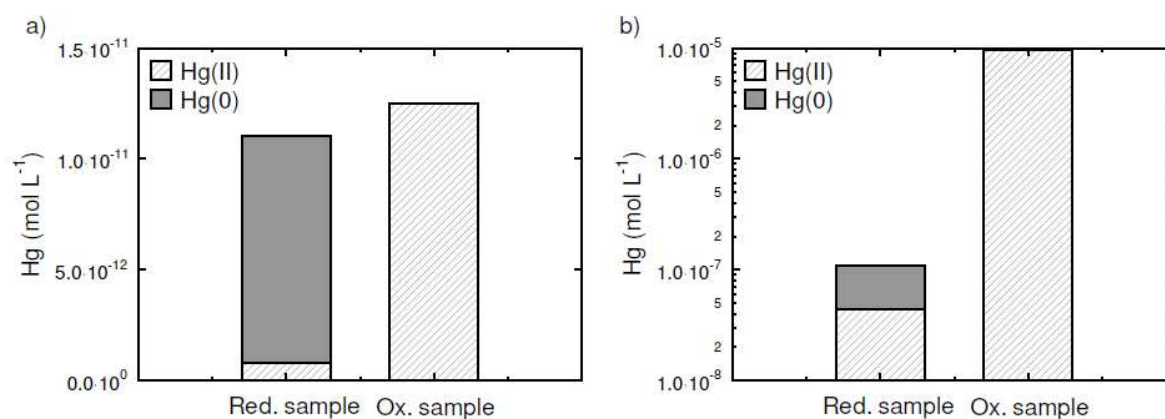


Fig. 5. Determination of the speciation of Hg after the retention experiment on the oxidized sample (AUB00976) and on the reduced sample (AUB00307). a. The initial Hg concentration was $8 \times 10^{-8} \text{ mol} \cdot \text{L}^{-1}$; b. the initial Hg concentration was $5.1 \times 10^{-5} \text{ mol} \cdot \text{L}^{-1}$. The lower the initial concentration, the higher the reduction percentage.

Table 1. Chemical extraction scheme for Hg fractionation highlighting the sequential extraction steps and mineralogical targets.

Step	Extractant	Mineralogical target
1	MgCl ₂ 1 M	Interlaminar exchange in clay minerals
2	Sodium acetate / Acetic acid (pH 5)	Calcite and clay edge sites
3	NH ₂ OH	Iron and manganese (oxyhydr-)oxides
4	H ₂ O ₂ 30 % + ammonium acetate (pH 2 at 85°C)	Organic matter

Table 2. Pore water chemistry measured after squeezing of the reduced sample (cations and anions in mmol·L⁻¹ and trace elements in μmol·L⁻¹).

Anions	Cl ⁻	SO ₄ ²⁻	S ₂ O ₃ ²⁻	Br ⁻	NO ₃ ⁻	PO ₄ ³⁻	F ⁻	
	1.47	26.02	0.20	0.002	< 0.016	0.018	0.034	
Cations	Si	Na	K	Mg	Ca	Ba	Sr	Fe
	0.2	2.78	1.38	16.87	16.57	< 0.002	0.42	< 0.005
Trace elements	As	B	Cd	Cr	Cu	Hg	Mn	Zn
	0.010	148	0.003	0.029	58	0.015	29	31

Table 3. Sorption and desorption coefficients calculated at the initial Hg concentration of 4.70 × 10⁻⁵ mol·L⁻¹ on the oxidized and reduced samples.

Sample	Hg _{added} (mol·L ⁻¹)	[Hg] _{final-sorp} (mol·L ⁻¹)	R _{SL} (kg·L ⁻¹)	R _d (L·kg ⁻¹)	[Hg] _{sorp-solid} (mol·L ⁻¹)	[Hg] _{final-desorp} (mol·L ⁻¹)	R _{d-desorption} (L·kg ⁻¹)
Reduced (AUB00307)	4.70 × 10 ⁻⁵	1.10 × 10 ⁻⁵	2.65 × 10 ⁻³	1.24 × 10 ³	3.60 × 10 ⁻⁵	5.58 × 10 ⁻⁷	2.40 × 10 ⁴
Oxidized (AUB00976)	4.70 × 10 ⁻⁵	3.74 × 10 ⁻⁵	2.58 × 10 ⁻³	9.98 × 10 ¹	9.61 × 10 ⁻⁶	3.41 × 10 ⁻⁶	7.06 × 10 ²